16th ICAAR LISBOA 2020-2022

16th International Conference on
Alkali-Aggregate Reaction in Concrete
Lisboa | LNEC | Portugal | 31 May - 2 June 2022

http://icaar2020-2022.lnec.pt

# Assessment of ASR damage to a heavily trafficked dual carriage concrete roadway in South Africa

**JP Kanjee [(1)], MG Alexander [(2)], Y Ballim [(1)]**

*(1) School of Civil & Environmental Engineering; University of the Witwatersrand, Johannesburg, South Africa, Janina.Kanjee@wits.ac.za, Yunus.Ballim@wits.ac.za*

*(2) Department of Civil Engineering; University of Cape Town, Cape Town, South Africa, mark.alexander@uct.ac.za*

## Abstract

*This paper reports on the diagnosis and rehabilitation strategy used to repair 11.2 kilometres of a dual carriageway concrete pavement forming part of a South African National Road (N2), near Somerset West in the Western Cape Province. Construction of the section of interest in this study took place between 1971 and 1972. The original design comprised of a 25 km span jointed unreinforced concrete pavement on a stabilised base. The pavement exhibited signs of serious ASR deterioration in 1986. Subsequently, the entire dual carriageway surface was sealed with a 14 mm stress-absorbing membrane interlayer (SAMI) in a bid to preserve the integrity of the pavement. A 40 mm Bitumen Rubber Asphalt Semi Open Graded (BRASO) mix was also overlaid on the concrete surface. However, by 2017, the road section exhibited transverse cracks through the asphalt overlay across all lanes, mimicking the underlying jointed concrete slabs. Cores were extracted from the dual carriageway trial section to evaluate the performance of the existing BRASO overlay and to assess the degree of ASR degradation.*

*The initial visual and optical examination of the concrete cores both highlighted the presence of cracked coarse aggregates in the mid-region of the concrete cores. The prognosis of deterioration of the concrete owning to ASR was confirmed using Tescan Integrated Mineral Analyse (TIMA) analysis, whereby the ASR gel was clearly identified and characterised in the aggregate crack veins. The $Na_2O_{eq}$ concentration was determined at depths of 25mm, 75mm, 125mm and 175 mm from the reference surface respectively. Residual expansion tests conducted were terminated hence the authors were unable to draw a conclusion on likely future expansion of the concrete. The rehabilitation strategy that was implemented to restore the integrity and riding quality of the composite pavement structure are also mentioned in this paper.*

***Keywords**: ASR; assessment; diagnosis; rehabilitation*

## 1. INTRODUCTION

Concrete is widely used in the construction of transport infrastructure (e.g. highways, airports runways, and bridge decks which is a key prerequisite for socio-economic development of any country [1], [2]. It is used in the construction of rigid pavements, is considerably more durable than other options such as bitumen and is less prone to deterioration such as rutting, cracking, stripping, loss of texture and development of potholes. Compared to flexible bituminous pavements, concrete pavements generally require little or no maintenance during their design life [3].

However, in recent years rapidly increasing heavy traffic coupled with chemical deterioration (in particular alkali aggregate reaction (AAR) has accelerated the deterioration of concrete pavements leading to the need for more frequent maintenance and repair actions than in the past. From a repair perspective, most studies [4]–[6] have focused on the performance of repair and rehabilitation alternatives, especially the application of overlays. Not much emphasis has been placed on comprehensive diagnosis of the mechanism and extent of deterioration of the concrete pavement in order to provide a better understanding of the material's performance. This knowledge will allow asset managers to understand the potential future performance of concrete pavements and thus make informed decisions with respect to scheduling maintenance and repair actions.

### 1.1 Background

Two forms of AAR are common in concrete viz alkali-carbonate reaction (ACR) and alkali-silica reaction (ASR). In ACR, the reaction is between the alkali's (sodium and potassium) and certain carbonate rocks, particularly calcite dolomite and dolomitic limestone present in some aggregates. In ASR which is the

most common form of AAR, the reaction occurs between alkalis and certain amorphous, disordered or poorly crystalized silica present in some aggregates such as opaline cherts and strained quartz [7]. It will only progress if all of the following three conditions are met viz sufficient quantity of reactive silica [8], sufficient concentration of alkalis in pore solution [9] and high moisture content (greater than 80% internal relative humidity) [10]. If all these conditions are met, a hygroscopic alkali-silica gel is formed which in the presence of moisture, expands and can exert swelling pressures that are sufficient to induce expansion and propagate cracking [11].

In South Africa, the first case of AAR was reported in the 1970's in the Cape Peninsula in the Western Cape province [12] but it can now potentially occur in other provinces including South Western Cape, Eastern Cape, Gauteng, Free-state, Kwa-Zulu Natal and Mpumalanga [13].

## 1.2 Plain Jointed Concrete Pavement (JCP)

In 1970, a 25 km span of dual carriageway was constructed as a plain Jointed Concrete Pavement (JCP), marking the first time concrete was used in the construction and development of road infrastructure in South Africa. The dual carriageway was part of the N2 National highway, between Cape Town and Somerset West in the Western Cape Province. At the time of construction, knowledge of the adverse effects of AAR in concrete was limited. In this case, the risk of AAR was as a result of the use of high alkali cement and a locally available greywacke stone as aggregate. Details of the actual concrete mix ingredients and proportions are not available in the published or non-published literature.

Five years after construction (i.e. in 1975), the pavement showed extensive surface cracking effectively reducing the stiffness of the pavement slab. An increase in surface crack widths was observed close to the joints where surface stresses are critical under traffic loading. The joints and cracking provided pathways for moisture ingress, which consequently increased the risk of abrasion, pumping (movement of underlying material through cracks in the pavement as a result of water pressure) and a loss of fines from the concrete. By 1980, minor structural failures developed in the vicinity of the transverse joints [14].

### 1.2.1 Initial Rehabilitation of plain Jointed Concrete Pavement

Investigations by the South African Department of Transportation [4] led to the adoption of a rehabilitation method in 1986 to repair of the structurally failed area in order to make provision for additional drainage pathways. The repair involved (i) the placement of a waterproof stress-absorbing chip-seal membrane interlayer (SAMI), and (ii) overlaying of a 40 mm Bitumen Rubber Asphalt Semi-Open (BRASO) graded mix over the chip-seal membrane [15].

However, in 2017, transverse reflective cracks propagated through the aged BRASO overlay at regular 4-meter intervals, across all the four lanes of the dual carriageway (as seen in Figure 1.1a and 1.1b). Additional cracking was seen to branch off the original reflective cracks and at numerous transverse joints (Figure 1.1a). Subsequently this resulted in asphalt being shoved in the wheel track. Reflective cracking was also noted around previously patched areas and at old joints (Figure 1.1b). Secondary effects of the cracking included a reduction in riding quality of the composite pavement structure [14].


Figure 1.1: a - Transverse reflective cracks propagated through the aged BRASO overlay at regular 4-meter intervals. b - Reflective cracking around previously patched areas and at old joints

Subsequent Rehabilitation of the plain Jointed Concrete Pavement

A consulting engineering firm (Royal Haskoning DHV) was appointed in 2017 to advise on the repair of a section of the pavement (11.2 km span), and recommended a rehabilitation approach which involved:

(i) milling and removing the 40 mm existing BRASO overlay and 14 mm Stress Absorbing Membrane Interlayer (SAMI);
(ii) thoroughly cleaning the exposed plain-jointed concrete surface to remove all loose material. Approximately 5-8 mm of the exposed JCP surface was finely milled and removed, and thoroughly cleaned again to remove all loose material before it was inspected to ascertain its integrity. In the instance where its integrity was compromised, the defective joints were repaired by partial depth repairs (concrete patching).
(iii) application of a bituminous tack coat on the concrete surface to promote bonding between the existing concrete and the overlay;

construction of a 50 mm Bitumen Rubber overlay proceeded by a 20 mm Ultra-Thin Friction Course (UTFC).

### 1.2.2 Characterization and evaluation of the degree of ASR degradation in the concrete pavement

In order to extent the service life of the concrete pavement, the focus (with respect to rehabilitation approach adopted) has been placed on employing different overlays. Little or no investigations have been undertaken to assess the condition of the existing concrete pavement. This vital information can be used to make informed decisions, with regard to the current state of the concrete and likely future behaviour of the material with respect to future ASR deterioration.

Prior to the second pavement rehabilitation, an initial investigation was conducted on cores extracted from the Dual Carriageway trial section to evaluate the performance of the existing BRASO overlay. Furthermore, the concrete pavement components of the cores were tested to characterise and evaluate the extent of ASR degradation. The remainder of the paper presents the relevant tests that were carried out on the concrete cores, as well as the findings.

## 2. EXPERIMENTAL METHODOLOGY

Six 150 mm diameter and five 100 mm diameter cores were extracted from the dual carriageway trial section (see Figure 2.1). It must be noted that this trial section was, and is still not subjected to traffic loading but was constructed using same concrete as that of the in-service highway which is adjacent to the trial section.


Figure 2.1: Google Earth image illustrating the 11.2 km span of the N2 route that was repaired and rehabilitated

The existing BRASO overlays on top of the concrete pavement (see Figure 2.2) were sawn off and tested. The scope of testing of the BRASO overlays and the results thereof are not within the scope of this paper.


Figure 2.2: Image of cores extracted from N2 Pavement comprising of 40mm Bitumen Rubber Asphalt Semi Open Graded (mix) overlay constructed on original the plain jointed concrete pavement

The remaining cores were sealed using plastic cling-wraps and stored in an environmental room at a temperature and relative humidity of, respectively, 23 °C and 50-60% prior to testing to diagnosis the nature and extent of ASR deterioration. Tests carried out included visual, petrographic, Tescan Integrated Mineral Analyser (TIMA), residual free alkali metal and residual expansion tests. The assessment criteria are summarized below:

- *Macroscopic inspection*: this was performed on the “as received” cores to for aspects such as size and distribution of aggregates, crack patterns and presence of ASR-gel, if any. The mass of each core was also measured.
- *Petrographic examination*: petrographic examination of thin concrete sections (27 x 46 x 0.03 mm) made from the cores was conducted in order to identify diagnostic features of ASR damage such as ASR gel and cracks radiating from reactive particles to the surrounding cement paste. This was done to corroborate the initial on-site ASR diagnosis of the concrete pavement. Petrographic images were taken using a digital Olympus DP74 camera attached to a light microscope.
- Tescan Integrated Mineral Analyzer (TIMA) analyses were conducted on the same thin concrete sections used in the petrographic analyses. The objective was to identify and characterise ASR gel presence in the concrete. TIMA technique uses a scanning electron microscope (SEM) with highly integrated Energy Dispersive X-Ray Analysis (EDX) system in its analyses.
- *Concentration of residual free alkali metals*: the concentration of residual free alkali metals present in the concrete pore solution is a key parameter in predicting the potential risk of ASR. The elemental profiles of the residual alkali metals in the concrete cores (aggregates and cement paste) were determined in accordance with the procedure outlined in the Cold Water Extraction method (CWE) [16]. Coarse aggregates were separated from the cement paste using the method proposed by Albayati and Johansson [17]. The cores were sawn into 50 mm increment discs (with the BRASO-concrete interface used as the zero depth reference point) as shown in Figure 2.3. The discs were then placed in a furnace at 600 °C for 7 hours and allowed to cool to room temperature. Coarse aggregates were thereafter dislodged from the cement paste using a hammer. The paste and aggregates were then milled to fine powder (< 80 µm) following the CWE method, and then sieved and stored in a desiccator with soda lime. The procedure outlined in the CWE method (with respect to leaching, filtration, dilution and acidification) was followed in order to obtain test solutions for the elemental concentrations of $Na^+$, $K^+$ and $Ca^{2+}$. A Spectroquant Pharo 300 machine was used to analyse the solutions for residual free alkali metals elemental concentrations.

- *Residual ASR expansion*: Residual expansion, which is a critical parameter in determining the severity of ASR deterioration with respect to monitoring ongoing and future expansion, was determined using the Quebec method [18]. The cores were placed standing in sealed plastic containers with > 95% RH which were then stored in a camber maintained at 38 °C. Expansion measurements were taken using a Demec gauge (gauge length = 100 mm) and by placing steel studs on three axis lines spaced at 120° apart longitudinally along on the cores. Specimen mass and temperature measurements in the chamber were also recorded.

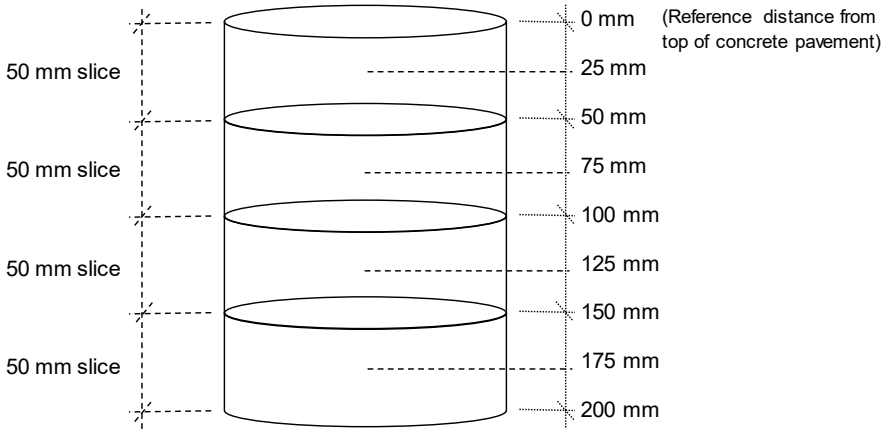


Figure 2.3: Schematic illustrating 50mm increments where cores were sawn, in preparation for the Cold Water Extraction method used to determine the free alkali metal content at various depths along the concrete core

# 3. RESULTS

## 3.1 Visual assessment of cores

An initial visual assessment of the concrete cores revealed that cracks were primarily present in the coarse aggregates. The cracks were typically orientated parallel to the BRASO overlay surface, with the maximum crack wide recorded being approximately 1.0 mm. A peculiar feature noted was that only the coarse aggregates primarily located in the mid-region of the concrete exhibited cracks as seen in Figure 3.1. No ASR gel was observed around the boundaries of the coarse aggregates.

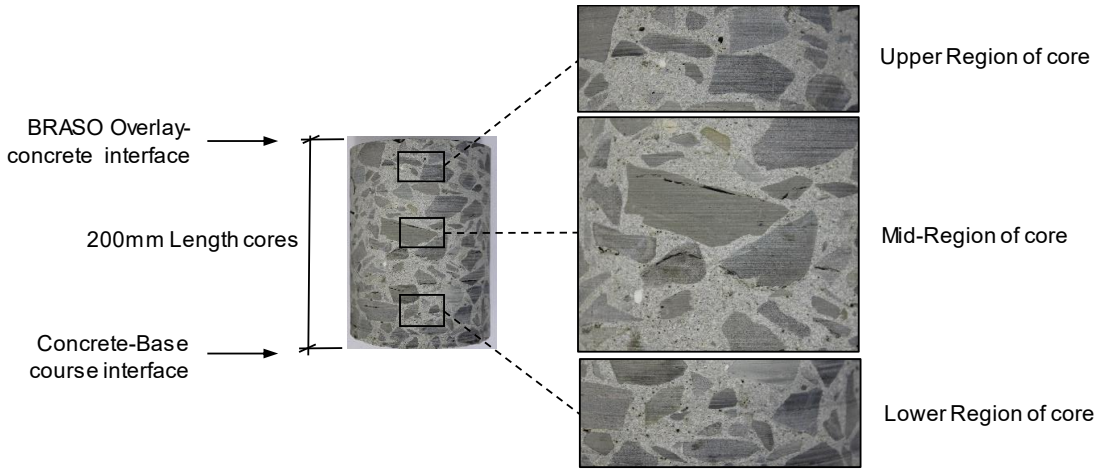


Figure 3.1: Images of the upper, mid and lower region of a concrete core illustrating the presence of cracks in coarse aggregates.

## 3.2 Petrographic analysis

Thin sections were produced from the upper, mid and lower region of the concrete cores. Figure 3.2 confirms the presence of cracking primarily present in the coarse aggregates which was more pronounced in the mid-region as noted in the initial visual assessment of the cores.

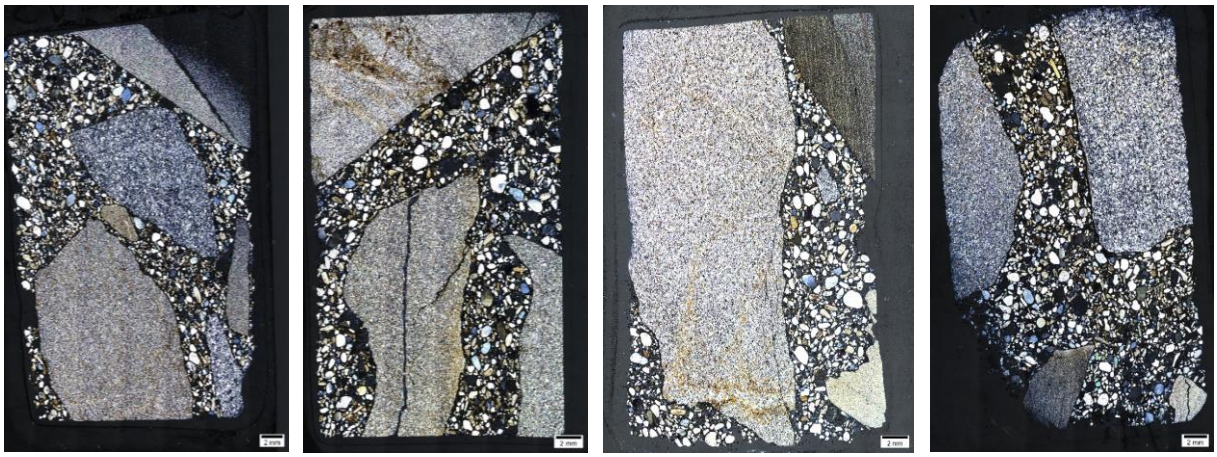

Upper Region of the core | Mid-Region of the core | Lower Region of the core

Figure 3.2: Images of thin section taken from the upper, mid and lower region of the concrete core, under crossed polarised light (scale bar = 2 mm (as shown at the bottom right of each image))

## 3.3 Tescan Integrated Mineral Analyser (TIMA) analysis

TIMA analyses of the thin sections revealed the primary phases present in the concrete. Furthermore elemental maps showing the presence and location of Si, Na and K were also obtained (Figure 3.3). The red vein running through the central aggregate was characterised as ASR gel (Gel 1) based on the EDX analysis which showed the percentage by mass of the chemical composition of the gel phase with respect to sodium, silicate, oxygen and potassium. This confirmed that the cracks present in the coarse aggregate are mainly as a result of gel expansion associated with ASR.

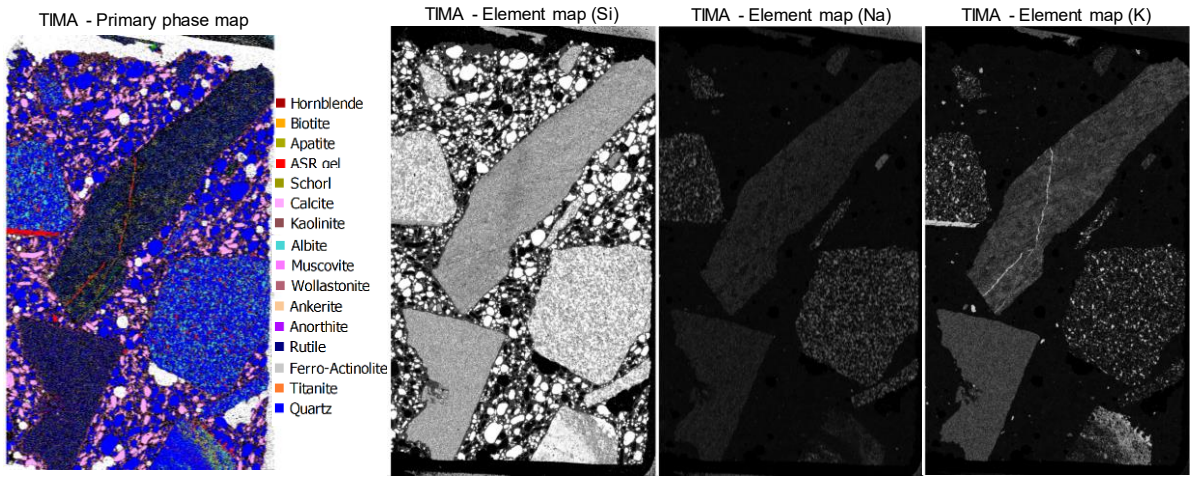


Figure 3.3: Primary phase and element map of a thin section using TIMA (View of field of each image is 21.0mm

A primary phase map of a sub-section (field of view: 4.5 mm) of the image presented in Figure 3.3 is shown in Figure 3.4. Two other types of ASR gels (Gel 2 and Gel 3) were identified and characterised in the aggregate crack veins. The chemical composition of Gel 2 and Gel 3 differed from Gel 1 as they contained traces of iron and chloride respectively.

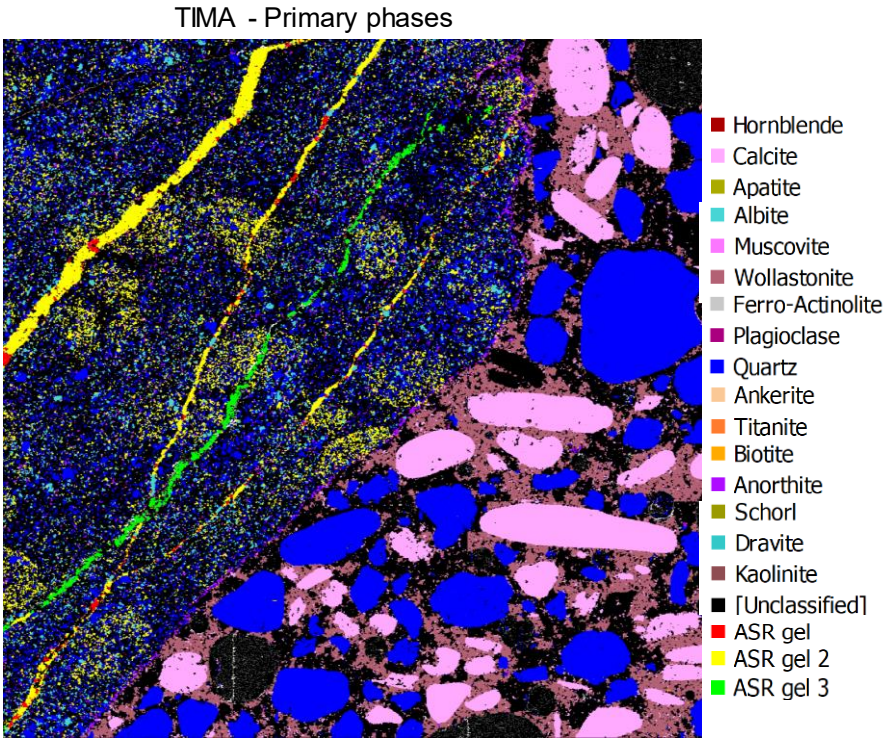


Figure 3.4: Primary phase map of a sub-section of a thin section using TIMA (View of field is 4.5mm)

## 3.4 Free Alkali Metal content

Table 3.1 presents the results of the free alkali metals content in the coarse aggregates using the CWE method. Figure 3.5 and Figure 3.6 show the residual free alkali metals ($Na^+$, $K^+$ and $Ca^{2+}$) profiles obtained for the cement paste using the CWE method. The data points cover the full length of the two cores tested (A and B) and were not been corrected to take into account the alkali contribution of the aggregates. Each data point represents the respective free alkali metal average value calculated from specimens A & B at a given depth, whilst the bar represents the maximum and minimum value that was obtained from specimens A & B, at a given depth.

Table 3.1: Free alkali metals content in the coarse aggregates

| Element | Quantity (mmol/kg) |
|---|---|
| $K^+$ | 6.7 |
| $Na^+$ | 11.5 |
| $Ca^{2+}$ | 58.0 |

As seen in Figure 9 the $K^+$ metal profile decreased at both the upper and lower depths (25mm and 175mm from the reference surface) of the core, in contrast to the $Na^+$ metal profile which decreased at the central depths (75mm and 125mm) of the core. These results do not support the work conducted by Plusquellec [19] that illustrate that typically both the $Na^+$ and $K^+$ metals profile follow the same trend i.e. both the $Na^+$ and $K^+$ concentration either stay constant or decrease at similar depths of the concrete. The decreasing trend is due to the consumption of both alkalis in the chemical reaction with the reactive silica, resulting in ASR gel.

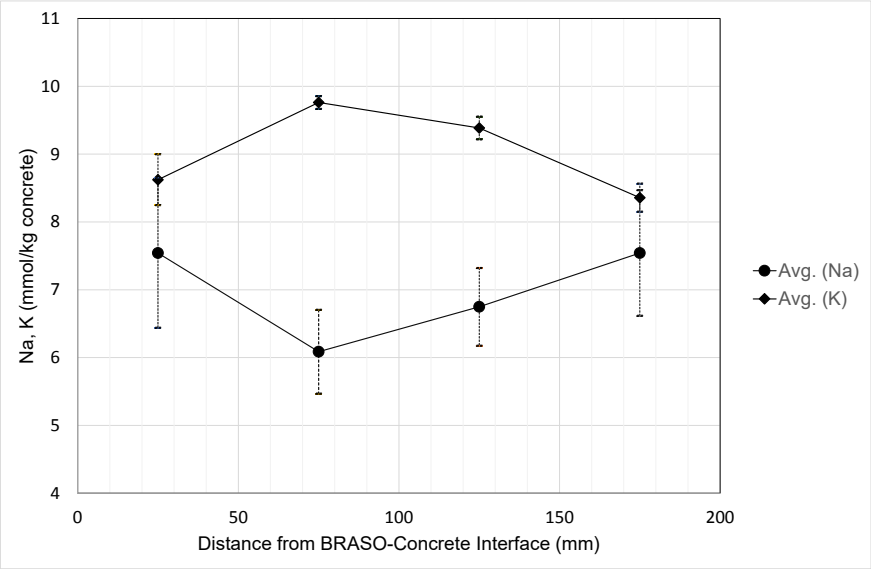


Figure 3.5: Variation of $Na^+$, $K^+$ profiles (mmol/kg) as a function of distance from reference surface

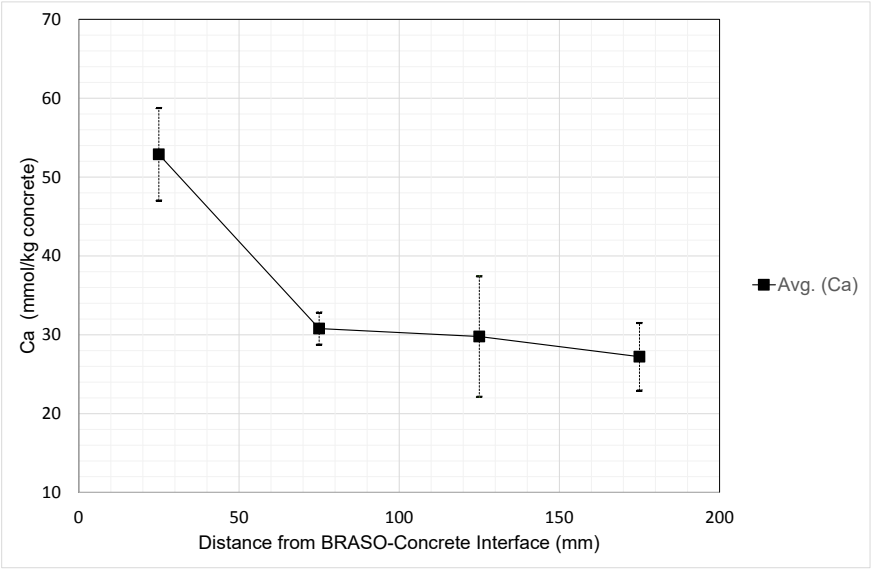


Figure 3.6: Variation of $Ca^{2+}$ profile (mmol/kg) as a function of distance from reference surface

The $Ca^{2+}$ metal profile decreased as the distance from the BRASO-concrete interface increased. The highest values of calcium content recorded was 59 mmol/kg. These high values can be attributed to the use of water when carrying out the cold water extraction method thus partially dissolving several of the hydrates. Gilles *et al*,. [19] recommend the use of used methanol instead of water for the cold water extraction to determinate the Ca content.

The $Na^+$ and $K^+$ metal contents (mmol/kg) were converted to $Na_2O_{eq,conc}$ (kg/m$^3$) using Equation 1:

$$Na_2O_{eq,conc} = \frac{M(Na_2O)}{2} \cdot (Na_{conc} + K_{conc}) \cdot \rho_{concrete} \quad \text{Equation 1}$$

where $\mathrm{Na_2O_{eq,conc}}$ is the alkali metal content obtained from the CWE method in kg/m$^3$, $\mathrm{M(Na_2O)}$ is the molar mass of $Na_2O$ (0.06198 kg/mol), $\mathrm{Na_{conc}}$ and $\mathrm{K_{conc}}$ are the $Na^+$ and $K^+$ contents of the sample expressed in mol/kg, and $\rho_{\mathrm{concrete}}$ is the concrete density in kg/m$^3$ (assumed to be 2400 kg/m$^3$). The $\mathrm{Na_2O_{eq,conc}}$ profile is presented in Figure 3.7.

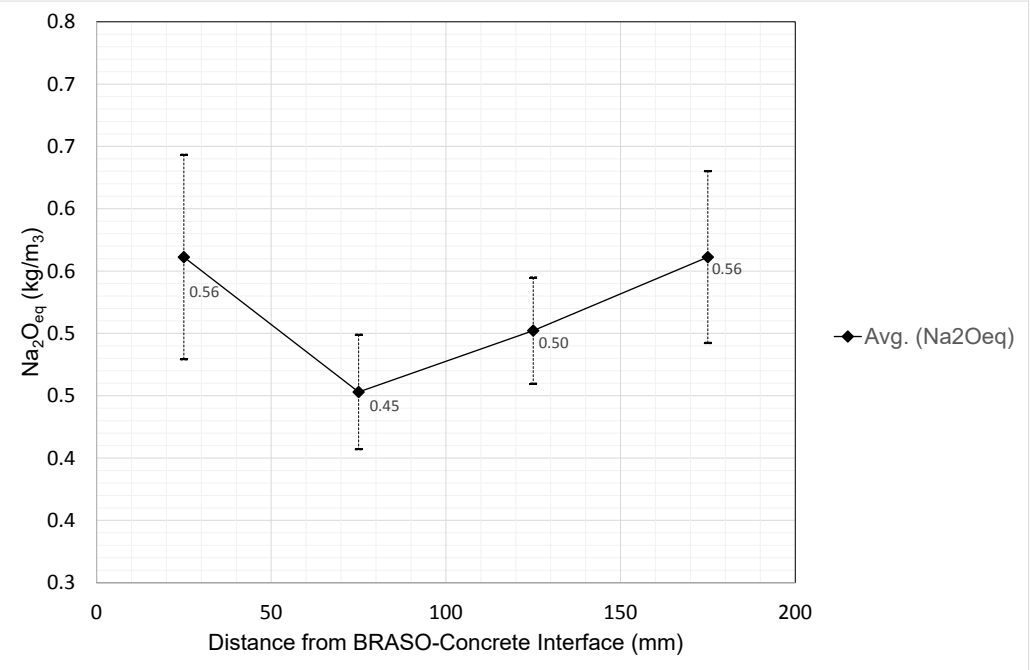


Figure 3.7:$Na_2O_{eq}$ (kg/m$^3$) profile across the full length of the cores A and B. The results have not been corrected for the contribution of alkali's from the aggregates.

It can be seen that at both the outer regions (top and bottom) at depths of 25 and 175 mm, the $\mathrm{Na_2O_{eq,conc}}$ is 0.56 kg/m$^3$ which is higher than in the mid-sections (75 and 125 mm) which have 0.45 and 0.50 $\mathrm{Na_2O_{eq,conc}}$ kg/m$^3$ respectively. The decrease in availability of alkalis in the mid-sections can be attributed to the consumption of Na and K in the pore solution which facilitates the development of ASR gel. This result is supported by the presence of ASR gel located in the cracked coarse aggregate in the mid-section of the core.

With regard to likely future ASR deterioration (assuming the presence of sufficient moisture and reactive silica in the concrete), the outer regions of the concrete exhibit a higher risk of future deterioration, with respect to the availability of $Na^+$ and $K^+$ to facilitate ASR.

## 3.5 Residual expansion

Figure 3.8 illustrates the initial longitudinal expansion measurements on core specimens C and D. Previous studies have indicated that strains recorded over the initial 8-week pre-conditioning period can be attributed to various mechanisms including (i) thermal expansion due to increased temperature (38 °C), (ii) moisture uptake resulting from the test chamber (> 95% RH) and drying of specimens prior to conducting the test, and (iii) stress release when specimens are tested too early after coring.

An average longitudinal expansion of 384 and 405 microstrain were recorded on cores C and D respectively, over the 8 week period. Longitudinal expansion measurements were then corrected to exclude the pre-conditioning period to account for the factors noted previously.

The subsequent rate of expansion dropped by 58% and 68% in cores C and D, when comparing the rate of expansion from the initial pre-conditioning period and the expansion exhibited post the initial 8 week pre-conditioning period. The residual expansion tests were terminated due to the lock-down imposed by CO-VID 19, no further data was obtained. The authors were unable to draw a conclusion on likely future expansion of the concrete.

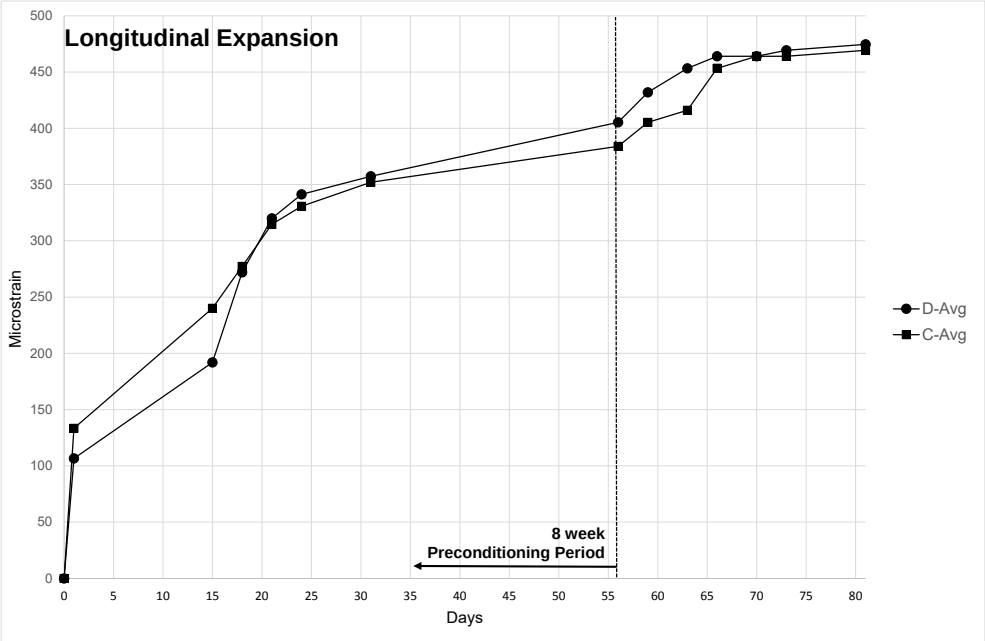


Figure 3.8: Longitudinal expansion measurements from expansion tests in air with >95 RH and 38°C

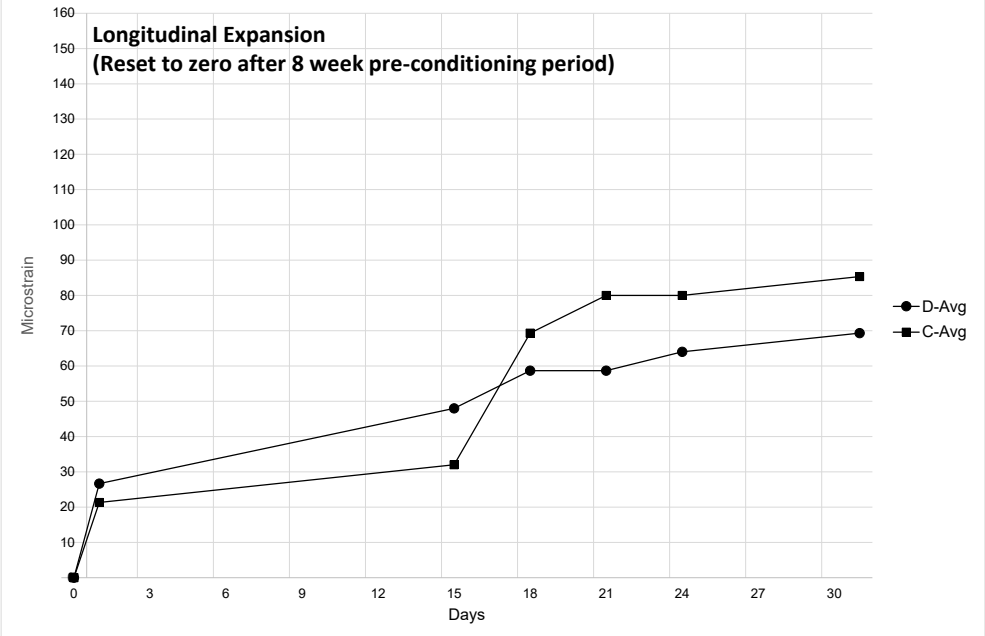


Figure 3.9: Corrected longitudinal expansion measurements from expansion tests in air with >95 RH and 38°C (excluding initial 8 week pre-conditioning period)

## 4. CONCLUSIONS

Five types of assessments (visual, petrographic, Tescan Integrated Mineral Analyser (TIMA), residual alkali metal and residual expansion tests) were carried out in order to assess the condition and extent of ASR deterioration in the concrete cores extracted from the N2 dual carriageway trial section.

The initial visual and optical examination of the concrete cores both highlighted the presence of cracked coarse aggregates in the mid-region of the concrete cores. No ASR gel was observed around the boundaries of the coarse aggregates. The prognosis of deterioration of the concrete owning to ASR was

confirmed using the TIMA analysis, whereby the ASR gel was clearly identified and characterised in the aggregate crack veins.

The determination of the free alkali metals ($Na^+$ and $K^+$) presented in the cement paste, was used to obtain the residual $Na_2O_{eq}$ concentration profiles. The results showed that $Na_2O_{eq}$ concentration at both the upper and lower regions of the core were 0.56 kg/m3, in comparison to the mid-region were the $Na_2O_{eq}$ concentration was 0.45 and 0.50 kg/$m^3$ (at depths of 75mm and 125m from the reference surface respectively). The decrease in $Na_2O_{eq}$ concentration could be attributed to the consumption of Na in the pore solution, facilitating the development of ASR gel and subsequent cracking of the coarse aggregates in the mid-region of the core.

The residual expansion results presented were preliminary. The test was terminated due to the lock-down imposed by CO-VID 19, no further data was obtained. The authors were unable to draw a conclusion on likely future expansion of the concrete.

In conclusion, none of results from the assessments conducted have provided evidence to explain in particular the prominent cracking of coarse aggregates in mid-region of the concrete owing to ASR deterioration. This phenomenon requires further investigation to determine the underlying cause in order to prevent further deterioration of the concrete in the upper and lower regions of the concrete.

## 5. ACKNOWLEDGMENTS

The authors would like to acknowledge the support of this work by the National Research Fund (NRF) of South Africa, Grant no. 113843.

## 6. REFERENCES

[1] E. Ivanova and J. Masarova, ‘Importance of road infrastructure in the economic development and competitiveness. Economics and Management’, Econ. Manag., vol. 18, no. 2, pp. 263–274, 2013.

[2] H. Wang, ‘Life-cycle analysis of repair of concrete pavements. Eco-Efficient Repair and Rehabilitation of Concrete Infrastructures’, in Woodhead Publishing Series, 2018, pp. 723–738.

[3] T. Smith and P. Maillard, ‘The Sustainable Benefits of Concrete Pavement’, in 42th Congrès annuel de l’AQTR Defi: Transport Durable, 2007.

[4] B. K. S. INC, ‘Experimental overlays of a distressed rigid pavement’, 1983.

[5] F. C Rust and A. W. Viljoen, ‘Evaluate the behaviour of experimental rehabilitation measures on the concrete road in the Cape N2’, 1984.

[6] O. Schnitter and V. . Francis, ‘Asphaltic rehabilitation of a distressed rigid pavement’, pp. 167–176, 1992.

[7] D. . Hobbs, Alkali–Silica Reaction in Concrete. Thomas Telford, London, 1988.

[8] Poole A.B, ‘The Alkali-Silica Reaction in Concrete’, R.N. Swamy Blackie and Son, Ed. London, 1992, p. 333.

[9] 221 ACI Committee, ‘State of the Art Report on Alkali Aggregate Reactivity’, ACI 221.1R-98, p. 31, 1998.

[10] C. Larive, A. Laplaud, and O. Coussy, ‘The role of water in alkali– silica reaction’, Proc. 11th Int. Conf. Alkali–Aggregate React. Concr. Que´bec City, vol. ed. by M.A, pp. 61–69, 2000.

[11] T. E. Stanton, ‘Expansion of concrete through reaction between cement and aggregate’, Proc. ASCE, vol. Vol 66, no. 10, pp. 1781–1811, 1940.

[12] Ekolu S. O, ‘Contribution to Diagnosis of Alkali-Silica Reaction in a Bridge Structure’, Orientations, pp. 597–602, 2009.

[13] M. Alexander and G. Blight, ‘Southern and Central Africa’, in Alkali-Aggregate Reaction in Concrete, I. Sims and A. Poole, Eds. CRC Press, Taylor and Francis Group, 2017, pp. 509–538.

[14] ‘Bitumen-rubber process in highways repairs.pdf’, Engineering news, Vol 6, No 23, 1986.

[15] P. Strauss, J. Heerden, and P. Molenaar, 'Using rubberized asphalt to rehabilitate an alkali-silica affected jointed concrete pavement', AsphaltNEWS, vol. 32, no. 3, pp. 8–13, 2018.

[16] G. Plusquellec, M. . Geiker, J. Lindgård, J. Duchesnec, B. Fournier, and Weerdt K. De, 'Determination of the pH and the free alkali metal content in the pore solution of concrete: Review and experimental comparison', Cem. Concr. Res., vol. 96, pp. 13–26, 2017.

[17] Y. Albayati and J. Johansson, 'Recycling of cement and aggregates from demolition concrete — A study of the effect on separation by thermal decomposition of concrete', CHALMERS, Göteborg, Sweden, 2017.

[18] B. Fournier, M. A. Be´rube´, K. J. Folliard, and M. Thomas, 'Report on the Diagnosis, Prognosis, and Mitigation of Alkali–Silica Reaction (ASR) in Transportation Structures', Fed. Highw. Adm. FHWA-HIF-09-004, 2010.

[19] G. Plusquellec, M. Geiker, J. Lindgård, and Weerdt K. De, 'Determining the free alkali metal content in concrete', Cem. Concr. Res., vol. 105, no. March 2018, pp. 111–125, 2018.

[20] I. Hager, 'Behaviour of cement concrete at high temperature', vol. 61, no. 1, 2013.